JARO 15: 31–43 (2014)
DOI: 10.1007/s10162-013-0419-7

JARO
Journal of the Association for Research in Otolaryngology

Research Article

Ouabain-Induced Cochlear Nerve Degeneration: Synaptic Loss and Plasticity in a Mouse Model of Auditory Neuropathy

Yasheng Yuan,[1,2] Fuxin Shi,[1,2] Yanbo Yin,[1,2] Mingjie Tong,[1,2] Hainan Lang,[3] Daniel B. Polley,[1,2] M. Charles Liberman,[1,2] and Albert S.B. Edge[1,2]

[1]*Department of Otology and Laryngology, Harvard Medical School, Boston, MA 02115, USA*
[2]*Eaton-Peabody Laboratory, Massachusetts Eye and Ear Infirmary, 243 Charles Street, Boston, MA 02114, USA*
[3]*Department of Pathology and Laboratory Medicine, Medical University of South Carolina, Charleston, SC 29425, USA*

Received: 10 March 2013; Accepted: 19 September 2013; Online publication: 10 October 2013

ABSTRACT

Ouabain application to the round window can selectively destroy type-I spiral ganglion cells, producing an animal model of auditory neuropathy. To assess the long-term effects of this deafferentation on synaptic organization in the organ of Corti and cochlear nucleus, and to ask whether surviving cochlear neurons show any post-injury plasticity in the adult, we quantified the peripheral and central synapses of type-I neurons at posttreatment times ranging from 1 to 3 months. Measures of normal DPOAEs and greatly reduced auditory brainstem responses (ABRs) confirmed the neuropathy phenotype. Counts of presynaptic ribbons and postsynaptic glutamate receptor patches in the inner hair cell area decreased with post-exposure time, as did counts of cochlear nerve terminals in the cochlear nucleus. Although these counts provided no evidence of new synapse formation via branching from surviving neurons, the regular appearance of ectopic neurons in the inner hair cell area suggested that neurite extension is not uncommon. Correlations between pathophysiology and histopathology showed that ABR thresholds are very insensitive to even massive neural degeneration, whereas the amplitude of ABR wave 1 is a better metric of synaptic degeneration.

Keywords: hair cells, ribbon synapse, neurodegeneration

INTRODUCTION

In recent years, several animal models of primary neural degeneration, i.e., loss of cochlear sensory neurons without concomitant loss of cochlear hair cells, have been described. One particularly powerful one was first discovered in the gerbil, where repeated application of ouabain to the round window membrane, designed as a means to cause strial atrophy, was instead seen to cause massive degeneration of the type-I spiral ganglion cells innervating the inner hair cells (Schmiedt et al., 2002), without significant loss of hair cells, and with preservation of hair cell function, at least as seen via otoacoustic emissions (Lang et al., 2005; Lang et al., 2008).

This neuropathic model has generated significant interest, mainly because of its utility in experiments designed to test the ability of transplanted neural progenitors to survive, grow, and re-innervate a denervated organ of Corti (Corrales et al., 2006; Lang et al., 2008; Chen et al., 2012). Such experiments could pave the way for cell-based therapies for auditory neuropathy, i.e., human hearing loss characterized by primary neural degeneration in the cochlea (Starr et al., 1996). For this type of transplantation experiment, the animal model should present with a cochlea completely devoid of endogenous sensory fibers, such that any post-transplantation synaptogenesis can be unambiguously ascribed to the transplanted progenitors.

Cochleas with primary neural degeneration are also useful for a completely different experimental

M. Charles Liberman and Albert S.B. Edge contributed equally to this work.

Correspondence to: Albert S.B. Edge • Eaton-Peabody Laboratory • Massachusetts Eye and Ear Infirmary • 243 Charles Street, Boston, MA 02114, USA. Telephone: +1-617-5734452; Fax: +1-617-7204408; email: albert_edge@meei.harvard.edu

line of inquiry. Although cochlear sensory cells and sensory neurons are both needed for normal hearing, it is difficult to tease apart the relative contributions of each to the complex perceptual changes that accompany sensorineural hearing loss because both elements are often damaged, or destroyed, together after cochlear insults. If the ouabain treatment could be titrated to create different degrees of partial cochlear neuropathy, without compromising hair cell function, the resultant changes in central auditory processing and/or auditory behavior could be very interesting to study.

Although several prior studies of the ouabain neuropathy model have carefully assessed the survival of spiral ganglion neurons (Lang et al., 2005), none has looked at the synaptic architecture of the cochlea or the cochlear nucleus after this type of insult, and a number of important questions remain. For example, is it possible to remove all cochlear nerve synapses in the inner hair cell area? Can the degree of synaptic survival be accurately predicted by cochlear function tests such as the auditory brainstem response? Do surviving cochlear neurons maintain a normal pattern of innervation, or do they extend processes and/or branch to begin re-innervating the (putatively undamaged) hair cells, as has been suggested in studies of acoustic injury (Lawner et al., 1997) and cochlear nerve transection (Spoendlin and Suter, 1976)?

To address these and other questions about the nature of the ouabain neuropathy model, and about the extent of post-injury plasticity in the adult cochlear nerve, we revisited the effects of ouabain in mouse with special attention to the synaptic architecture of its peripheral and central projections.

MATERIALS AND METHODS

Animal Groups and Surgery

Experiments were performed on female CBA/CaJ mice, aged 8–10 weeks. Unilateral cochlear denervation was accomplished by application of ouabain solution to the round window niche, as described previously (Lang et al., 2011). Animals were anesthetized with ketamine (100 mg/kg, i.p) and xylazine (10 mg/kg, i.p). Half the initial dose was given as a booster when needed. A posteroinferior skin incision was made in the retroauricular area of the right ear. The underlying muscles and facial nerve were separated by blunt dissection to expose the middle compartment of the bulla, and the round window niche was exposed through a small opening. Ouabain (1–2 μl, 1 mM in distilled water) was applied to the round window membrane for 10 min using a 10 μl Hamilton syringe, and then wicked off and exchanged for a fresh solution every 10 min for 1 h. The bulla was covered with muscle and fascia, the incision was closed with nonabsorbable suture, and the animal was transferred to a homeothermic blanket at 39.8 °C for the recovery period. Animals underwent cochlear function tests before, and 1 week, 1 month and 3 months after ouabain application; the left ear served as an untreated control. All procedures were approved by the institutional animal care and use committee of the Massachusetts Eye and Ear Infirmary.

Cochlear Function Tests

Auditory brainstem responses (ABRs) and distortion product otoacoustic emissions (DPOAEs) were recorded as described previously. Mice were anesthetized as described above. ABR stimuli were 5-ms tone pips with a 0.5 ms rise–fall time delivered at 30/s. Sound level was incremented in 5-dB steps, from 10 dB below threshold to 90 dB sound pressure level (SPL). Threshold for ABR was defined as the lowest stimulus level at which a repeatable morphology could be identified in the response waveform. DPOAEs were recorded for primary tones with a frequency ratio of 1.2 and with the level of the f2 primary 10 dB less than f1 level, incremented together in 5-dB steps. The 2f1–f2 DPOAE amplitude and surrounding noise floor were extracted. Threshold for DPOAEs is defined as the f1 level required to produce a response amplitude of 0 dB SPL.

Tissue Processing and Immunostaining

Cochleas were dissected and immediately perfused through the round window and oval window with 4 % paraformaldehyde in phosphate-buffered saline at pH 7.4. Cochleae were post-fixed in the same solution for 2 h at 4 °C. Some cochleas were decalcified (0.1 M EDTA), and embedded in OCT for frozen sectioning. Others were dissected into half-turns for whole-mount processing. Immunostaining began with a blocking buffer (PBS with 5 % normal goat or donkey serum and 0.2–1 % Triton X-100) for 1 to 3 h at room temperature and followed by incubation with some combination of the following primary antibodies: (1) rabbit anti-CtBP2 (BD Biosciences) at 1:100, (2) chicken anti-high molecular weight neurofilament (Millipore) at 1:500, (3) mouse anti-parvalbumin3 (Swant) at 1:300, (4) mouse anti-vGLUT1 (NeuroMab) at 1:200, (5) goat anti-Na/K ATPase α3 (Santa Cruz Biotechnology) at 1:200, (6) mouse anti-TuJ antibody (Bioscience Research Reagents) at 1:500, (7) mouse anti-GluR2 (Millipore) at 1:2,000, or (8) mouse anti-PSD-95 (NeuroMab) at 1:50. Primary incubations were followed by 2 sequential 60-min incubations at 37 °C in species-appropriate secondary

antibodies (coupled to Alexa Fluor dyes) with 1 % Triton X. Nuclear staining was performed with DAPI.

Image Acquisition and Morphometric Analysis

Cochlear Synapses

For cochlear whole mounts, piece lengths were measured in each case, and converted to cochlear frequency (Muller et al., 2005). Confocal z-stacks from each ear were obtained in the inner hair cell (IHC) and outer hair cell (OHC) area using a high-resolution glycerin-immersion objective (63×) and ×3.18 digital zoom and a 0.25 µm z-spacing on a Leica SP5 confocal microscope. For each stack, the *z*-planes imaged included all synaptic elements in the *x*–*y* field of view. The field of view for each stack encompassed ~10 IHCs, or ~11 OHCs from each row. Image stacks were ported to image-processing software (Amira, Visage Imaging), where synaptic ribbons, glutamate-receptor patches, and hair cells were counted using the "connected components" feature of the Amira software. Juxtaposition of ribbons and receptor patches was assessed by high-magnification reimaging of all the synaptic elements in each z-stack as an array of thumbnail projections, each centered on the *x*, *y*, *z*, coordinate of an element identified in the Amira analysis (Liberman et al., 2011).

Spiral Ganglion

Counts of spiral ganglion neurons (SGNs) were made in confocal images of mid-modiolar sections (14-um thickness) through Rosenthal's canal, immunostained with anti-TuJ antibodies. The cochlear frequency correlate of each half-turn visible in these mid-modiolar sections was determined as described previously (Stankovic et al., 2004). In each case, the total number of SGNs was counted in three mid-modiolar sections through Rosenthal's canal.

Cochlear Nucleus

For assessment of the cochlear nucleus, where volume, neuronal counts, and auditory nerve terminals were all quantified, frozen coronal brainstem sections (40 um) were cut through the ventral cochlear nucleus (VCN) and either Nissl-stained (for VCN area measures) or immunostained for neurofilament to count VCN neurons, or VGLUT1, a vesicular glutamate transporter, to assess auditory nerve central terminals (Zhou et al., 2007). For all these analyses, the VCN and its major subdivisions (AVCN and PVCN) were demarcated. The rostrocaudal extent of the VCN was determined in each case, and the sections at the middle of that extent were chosen for quantification. Low (×20 objective) and high (×63 objective) power images were transferred to MetaMorph software for analysis. For quantification of auditory nerve terminals, high-power images were used; the summed pixel intensity in the VGLUT1 channel was normalized with respect to an analogous image from a negative control section (processed without primary antibody) and then divided by the image area.

RESULTS

Cochlear Function Tests

Several prior studies (Schmiedt et al., 2002; Lang et al., 2005; Lang et al., 2008) have shown that ouabain application to the round window area can cause dramatic attenuation of cochlear neural responses, such as the ABR or the compound action potential, without significantly affecting responses that do not require cochlear synaptic transmission, such as the DPOAEs.

In the present study, one aim was to produce a pure and complete cochlear neuropathy, i.e., to maximize cochlear nerve loss throughout the cochlear spiral without causing any loss of, or damage to, the hair cells. One week after a 60-min application of 1 mM ouabain to the round window in mice, DPOAE thresholds, and suprathreshold amplitudes, are minimally affected, except at the highest stimulus frequencies (Fig. 1A, B). In contrast, ABR thresholds are shifted at all frequencies by at least 30–40 dB (Fig. 1C).

These measures of ABR threshold shift are significant underestimates for two reasons. First, in some cases, there is no measurable response at the highest stimulus levels presented (80 dB SPL), and a value of 80 dB is included in the average when this occurs. Second, at high SPLs, the ABR wave 1, classically considered to represent the summed activity of auditory nerve fibers (ANFs), may also include a robust contribution from inner hair cell receptor potentials that is difficult to exclude from the "threshold" analysis based on latency alone. As evidence of its non-neural origin, this putative IHC contribution, which appears as a shoulder on the rising phase of wave 1 (1A in Fig. 1D), is identical in mean waveforms computed from control and ouabain-treated ears: data for 16 kHz and 80 dB SPL are shown in Figure 1D. Prominent deflections at these early latencies were present at ABR "threshold" in two of the six cases included in Figure 1C (post-ouabain).

Cochlear Histopathology

Prior studies, mostly in gerbil, have also shown that round-window ouabain can remove virtually all the spiral ganglion cells (SGCs), the cell bodies of ANFs, while largely sparing the hair cells they synapse with (Schmiedt et al., 2002; Lang et al., 2005; Corrales et al., 2006). As shown in Figure 2, the same near-complete

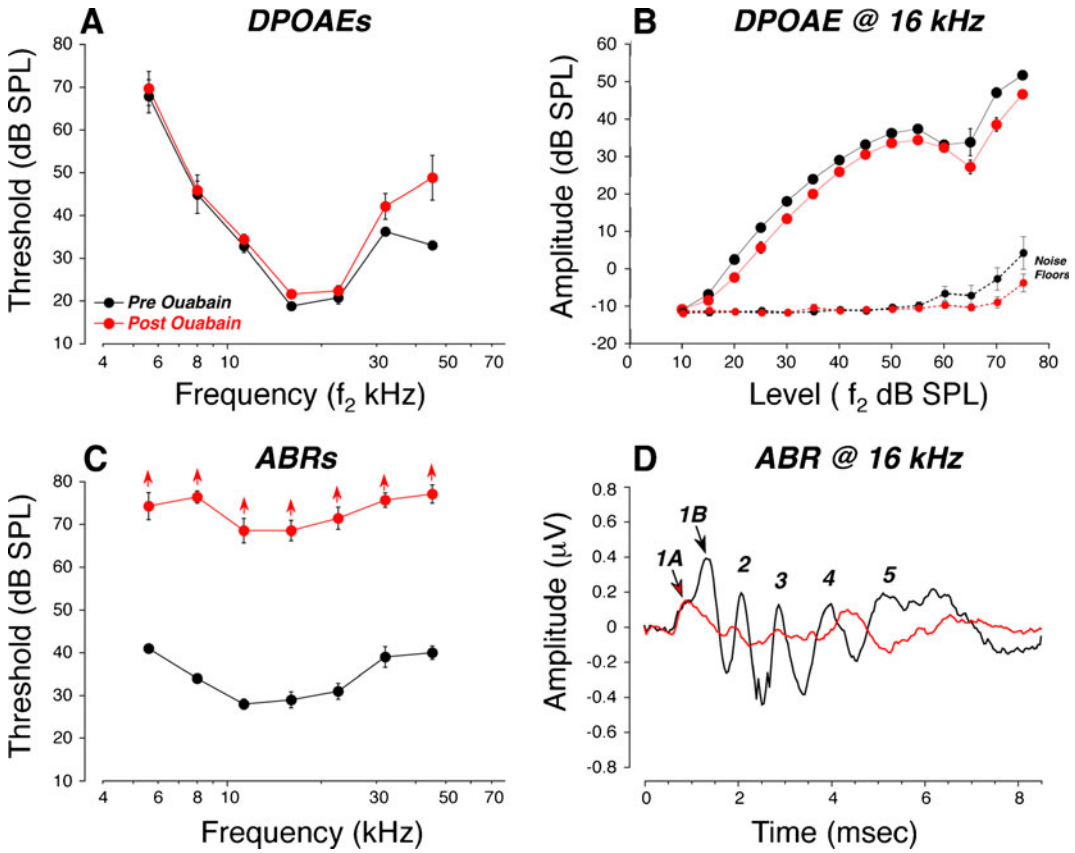

Fig. 1. Ouabain treatment can elevate ABR thresholds without significant changes in DPOAEs. **A** Mean DPOAE thresholds (±SEMs) for control ears (n=6) versus ears (n=6) tested 1 week after ouabain application. **B** Mean amplitude versus level functions for f_2=16 kHz for the same animals shown in panel **A**, with mean noise floors shown by *dashed lines*. **C** Mean ABR thresholds for the same animals shown in panel **A**. *Up arrows* on post-ouabain data indicate that thresholds are underestimated because in two ears, no response was detected at the highest level presented (80 dB SPL). **D** Mean ABR waveforms in response to 16 kHz tone pips at 80 dB SPL for the same animals shown in **A** and **B**. Waves *1–5* are indicated. See text for the significance of the wave *1A-1B* distinction. Key in **A** applies to all panels.

elimination of SGCs, without loss of inner or outer hair cells, can be achieved in the mouse.

However, as can be seen in Figure 2B (red arrow), and as noted in all prior studies, a small number of SGCs remain, roughly 5 % in all cochlear locations (Fig. 2C). None of the prior studies have evaluated whether the synapses between the few remaining SGCs and the denervated hair cell targets are altered. Plasticity in the branching and synaptic architecture of auditory neurons, even in the adult organ of Corti, has been suggested by prior studies of neuronal architecture after acoustic injury (Lawner et al., 1997). To study the synaptic alterations in the organ of Corti, we immunostained cochlear whole mounts with several immunomarkers as follows: (1) CtBP2, a major component of the presynaptic ribbon (Khimich et al., 2005); (2) GluA2, an AMPA-type glutamate receptor expressed by the postsynaptic terminal (Matsubara et al., 1996a; Frank et al., 2010; Liberman et al., 2011); (3) PSD-95, a component of the postsynaptic density at glutamatergic synapses (Opazo et al., 2012); and/or (4) neurofilament, a marker for afferent and efferent neuronal processes in the organ of Corti.

In the normal mammalian cochlea, each type-I ANF terminal contacts a single IHC via a single unbranched peripheral terminal, forming a discrete synaptic zone with a single presynaptic ribbon opposite a single postsynaptic active zone expressing glutamate receptors (Liberman, 1982; Matsubara et al., 1996b; Liberman et al., 2011). In mouse, each IHC is contacted by roughly 10–20 ANFs depending on cochlear location (Stamataki et al., 2006; Kujawa and Liberman, 2009; Meyer et al., 2009), and 95 % of ANF terminal show both a presynaptic ribbon and a postsynaptic density, while only ~5 % show a postsynaptic density without a presynaptic ribbon (Stamataki et al., 2006). In confocal z-stacks through the IHCs from a normal cochlea, synapses can be seen as closely juxtaposed pairs of ribbons (red) and receptor patches (green) studding the basolateral membrane of the IHC throughout the subnuclear zone (Fig. 3A top). There appear to be few, if any, unpaired ribbons or receptor patches; however, an accurate analysis requires higher-power images (see below). Neurofilament staining (Fig. 3A middle) reveals the dense meshwork of neuronal processes under the IHCs,

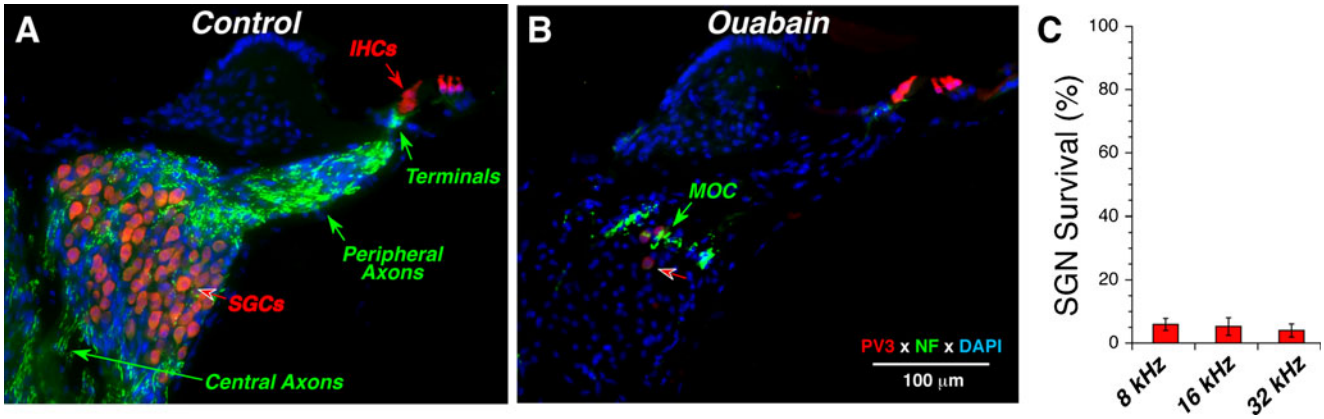

Fig. 2. Ouabain treatment can eliminate 95 % of spiral ganglion cells (*SGCs*) while sparing the inner and outer hair cells. Parvalbumin3 (*PV3*: *red*) was used as an immunomarker for SGCs and hair cells, and anti-neurofilament (*NF*: *green*) was used to label the auditory nerve fibers (*ANFs*). In the normal ear (**A**), anti-NF shows the myelinated central and peripheral axons of ANFs as well as their unmyelinated terminals under the inner hair cells. In the ouabain-treated ear (**B**), only a few SGCs remain (*red arrow*) and the anti-NF shows mostly medial olivocochlear (*MOC*) neurons in the intraganglionic spiral bundle (*green arrow*). Sections are from the upper basal turn; ouabain treatment was 1 week prior to histological processing. *Scale bar* in **B** applies to both panels. **C** Spiral ganglion cell survival at 1 week post ouabain. Cell counts from ouabain-treated ears (n=6) are normalized to place-matched counts from control ears (n=6). Data are from ears selected to have near-normal DPOAEs and ABR thresholds near, or above, 80 dB SPL, as shown in Fig. 1.

which includes radially directed terminals of spiral ganglion cells, and spiraling fibers of the lateral and medial olivocochlear (MOC) efferent systems. Merging all three markers (Fig. 3A bottom) shows the appositions among all three elements of the afferent synapse (e.g., at the white arrows).

In the ouabain-treated cochlea, there is a dramatic reduction in the number of ribbons and glutamate receptor patches in the IHC area (Fig. 3B top). Many remaining ribbons appear to be unpaired with glutamate receptor patches (e.g., red arrow), and, rarely, an orphan receptor patch is also seen (green arrow). The neurofilament staining (Fig. 3B middle) shows a corresponding lack of ANF terminals; however, the meshwork of spiraling fibers remains in the inner spiral bundle under the IHCs, and the thick tunnel-crossing fibers of the MOC system appear undiminished in number. The merged image (Fig. 3B bottom) suggests that many of the orphan ribbons are far from any neural processes (e.g., red arrow), although caution is needed since the neurofilament staining may not invade the most distal 1–2 μm of the terminal bouton.

To more accurately distinguish putative synapses (paired pre- and postsynaptic elements) from orphan (unpaired) synaptic elements in normal and ouabain-treated ears, the confocal z-stacks were reimaged as arrays of high-power "thumbnails." As illustrated in Figure 4A, each thumbnail in the array displays the voxel space immediately around a single ribbon (or receptor patch). Such thumbnail arrays are easily scanned to count synapses (and orphan elements) in each z-stack. Based on this analysis, ouabain clearly reduces the number of IHC synapses throughout the cochlear spiral (Fig. 4B), with a trend towards greater deafferentation at the basal end. Synaptic numbers continued to decline with posttreatment survival, such that, by 3 months, the numbers were essentially zero at the basalmost location sampled. At all cochlear regions, there were numerous orphan ribbons in the ouabain-treated ears; 70–90 % of ribbons were unpaired with a glutamate receptor patch, compared to <5 % in control ears, and the prevalence of orphan ribbons also increased with posttreatment survival (data not shown).

Examination of confocal z-stacks immunostained for a Na/K ATPase expressed by ANF terminals in the IHC area (McLean et al., 2009) suggests that ouabain treatment elicits plasticity in synaptic architecture in addition to simple degeneration of synaptic elements. Most dramatic is the appearance of large nerve terminals (e.g., Fig. 5D) near the apical ends of the hair cells; whereas normal ANF terminals never extend above the level of the IHC nucleus (Fig. 5B), these aberrant giant terminals in ouabain-treated ears often extend close to the cuticular plate (green arrows in Fig. 5D). Such ectopic terminals were clearly visible in ~80 % (34/44) of the z-stacks examined at the 8 and 16 kHz regions, and in ~40 % (16/44) of the z-stacks at the 4 and 32 kHz regions. They were equally common at 1 and 4-week survivals.

These aberrant terminals were generally not apposed to presynaptic ribbons. To better assess whether they form ribbon synapses with the IHCs, we immunostained four ouabain-treated ears for PSD-95, a postsynaptic marker for glutamatergic synapses (Opazo et al., 2012), along with neurofilament antibodies and the ribbon marker (anti-CtBP2). The neurofilament staining clearly reveals the aberrant nature of the remaining fibers in the IHC area; in the

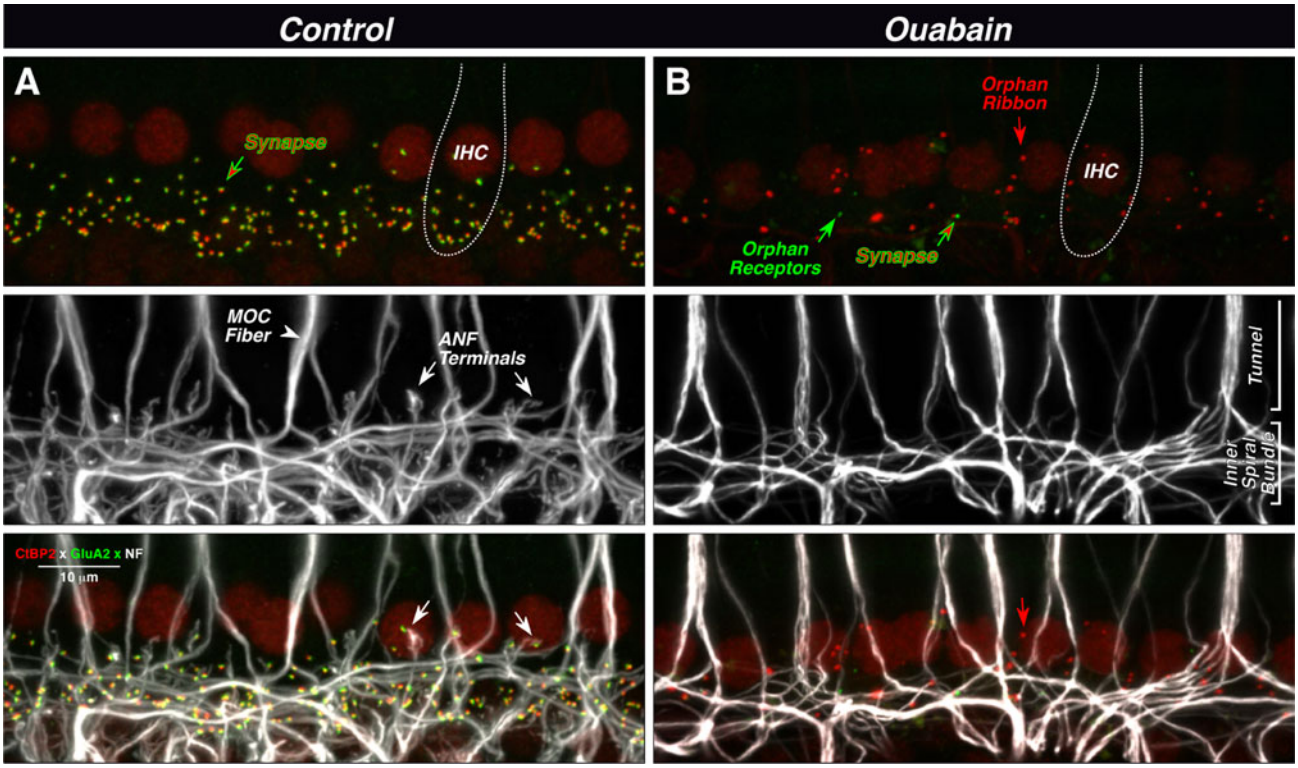

Fig. 3. Ouabain can eliminate virtually all synapses between auditory nerve fibers (*ANFs*) and inner hair cells (*IHCs*), as seen in maximal projections of confocal z-stacks. In the normal ear (**A**), each synapse (*top panel*) is a juxtaposed pair of *red* (anti-CtBP2) and *green* (anti-GluA2) puncta, showing the presynaptic ribbon and the postsynaptic receptor patch, respectively. IHC nuclei are also faintly stained (*red*), and the rough outline of one IHC is shown (*dotted line*). Unmyelinated processes of ANFs and medial olivocochlear fibers (*MOC*) are stained with anti-neurofilament antibodies (*middle panel*). MOC fibers project to outer hair cells outside the field of view. In the merge view (*bottom panel*), the juxtaposition between ANF terminals and synaptic puncta is evident (see *white arrows*). In the ouabain ear (**B**), only one synapse remains (*red-green arrow*) among these ten IHCs. There are numerous orphan ribbons (e.g., *red arrow*) and two orphan receptor patches (e.g., *green arrow*). The merged view (*bottom panel*) suggests that these orphan elements are not paired with ANF terminals (e.g., *arrows*). Images are from the 32 kHz region; *scale bar* in **A** (merge) applies to all panels.

normal ear (Fig. 6A), the terminal branches of type-I afferent neurons are relatively thin and short, and each ends very near a closely juxtaposed pair of CtBP2- and PSD-95-positive puncta. In the ouabain-treated ear (Fig. 6C), the terminals are longer, thicker, and tend to wrap around and between the IHCs. When viewed in 3-D, we rarely saw an aberrant terminal in close proximity to a ribbon, and never saw closely apposed PSD-95 and CtBP2 puncta, near one of these aberrant fibers; the apparent proximity of terminals and puncta in Figure 6C arises because the image is a maximum projection from ten adjacent IHCs.

The images in Figures 5 and 6 also suggest that ouabain treatment causes an increase in ribbon size (red arrows in Figs. 5D and 6C) and migration of orphan ribbons to the perinuclear region (e.g., Figs. 5C, D and 6C). To more systematically assess the rearrangement of synaptic profiles in the ouabain-treated ears, we measured the positions of all synaptic elements, *re* the IHC's basal pole, in large number of IHCs from the 16-kHz region (Fig. 7). In the normal ear, synapse position follows a roughly Gaussian distribution centered ~10 µm from the basal pole, and the small number of orphan ribbons are distributed similarly throughout the subnuclear cytoplasm (Fig. 7B). In the ouabain-treated ear, orphan ribbons, which are now in the majority, appear normally distributed re the IHCs basal pole (Fig. 7D, black), but synapses are now clustered nearer the basal pole (Fig. 7D red and 5B). There is also an increase in the number of large ribbons (>800 voxels) at all positions along the IHCs long axis (Fig. 7C). Only the relative size of the ribbons is important, since the absolute size is greatly distorted by the point-spread function of the confocal imaging system.

In contrast to the massive degeneration of type-I ganglion cells and their IHC synapses, the effects of ouabain on type-II neurons and their OHC synapses are minimal (Fig. 6B, D). In the ouabain-treated ears, ribbon counts are indistinguishable from normal (Fig. 4C), except for a slight reduction at the base of the cochlea, where the DPOAE data suggest there is some OHC

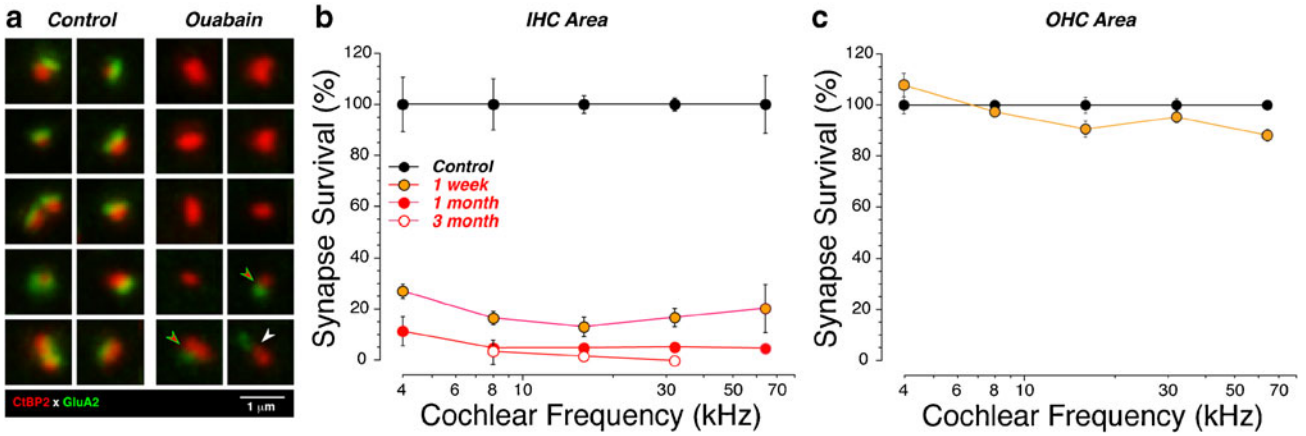

Fig. 4. Synaptic counts in control and ouabain ears show the massive deafferentation in the IHC area compared with minimal change in the OHC area. **A** High-power confocal thumbnails of all synaptic elements are used to assess whether ribbons are orphan or paired with a receptor patch. In this sample of ribbons from the IHC area, all those in the control columns are paired, whereas only three from the ouabain column are paired (*arrows*), and in one of those (*white arrow*), the two elements are abnormally far apart. **B** Group means (±SEMs) for synapse survival on IHCs; group sizes were *control* three ears from three animals, *1 week* four ears from four animals, *1 month* six ears from six animals, and *3 months* six ears from six animals. Data are expressed as a percentage of the mean control data. All ouabain-treated ears had ABR threshold shifts of at least 30 dB; however, the shifts were smaller than those for ears with ganglion cell counts (Fig. 2C). In each cochlear region from each animal, the count is derived from ~20 IHCs, i.e., two confocal z-stacks such as those shown in Figure 3. **C** Group means (±SEMs) for synapse survival on OHCs, averaged over all three rows; group sizes for both were four ears from four animals. In each cochlear region from each animal, the count is derived from ~65 OHCs. Data are expressed as a percentage of the mean control data. All ouabain-treated ears had ABR threshold shifts of at least 30 dB and showed synaptic losses in the IHC area exceeding 95 %, except at 4 kHz where the mean losses were 90 %. Key in **B** also applies to **C**.

damage (Fig. 1A). Absolute OHC ribbon counts, averaged over all five cochlear regions evaluated, were 2.30/OHC (±0.07 SEM) in normal ears compared with 2.24/OHC (±0.07 SEM) in ouabain-treated ears.

As seen in the confocal *y–z* projections, the normal OHC (Fig. 6B) has a cluster of ribbons near the basolateral pole of the OHC, and other ribbons scattered in supranuclear regions. In contrast to the normal IHC area, where virtually every presynaptic ribbon is paired with a PSD-95 patch, most OHC ribbons are unpaired, even in the normal ear (Fig. 6B). Synapses, i.e., closely juxtaposed pairs of PSD-95 and CtBP2 puncta, were seen only in the subnuclear region, in both normal and ouabain-treated ears (red-green arrows in Fig. 6C, D). Absolute synaptic counts, averaged over all cochlear regions evaluated, were 0.066/OHC (±0.012 SEM) in normal ears compared with 0.056/OHC (±0.012 SEM).

Cochlear Nucleus Histopathology

The central axons of ANFs branch to innervate cells in the VCN and the dorsal cochlear nucleus. The central projections of ANFs can be identified in the VCN by virtue of their expression of a vesicular glutamate transporter (VGLUT1) that is not expressed by cochlear nucleus terminals from other sources (Zhou et al., 2007). To quantify the loss of ANF central projections, we immunostained frozen sections through the VCN for VGLUT1 (Fig. 8A, B). To visualize and count the somata of VCN neurons, we also stained for a general neuronal marker (neurofilament).

As seen in Figure 8C, the loss of VGLUT1 staining was significant in the ouabain-treated ears. Comparison to the data on loss of SGCs (Fig. 2) suggests that ANF terminal degeneration in the VCN ultimately reaches the same degree of completeness as the loss of SGCs would predict, but with a slightly slower time course. The analysis of cochlear nucleus histopathology also revealed a more modest, but highly significant reduction in overall VCN cross-sectional area and neuronal counts (Fig. 8D, E).

Correlations Between ABR Metrics and Cochlear Neuropathy

The ouabain-treated cases included in the mean data for Figure 1, and for the synaptic counts in Figure 4, were selected to include only those with minimal DPOAE threshold shifts. Despite considerable care to deliver precisely the same drug volume for precisely the same period of time, some ouabain-treated animals showed significant DPOAE threshold elevations; such ears were not included in this study

To test the reliability of different ABR metrics in predicting the degree of neuropathy in animals without hair cell damage, we counted IHC synapses in six ouabain-treated cases with significant (>30 dB) ABR shifts and two ouabain-treated cases with minimal (<15 dB) ABR threshold shifts; all eight cases had

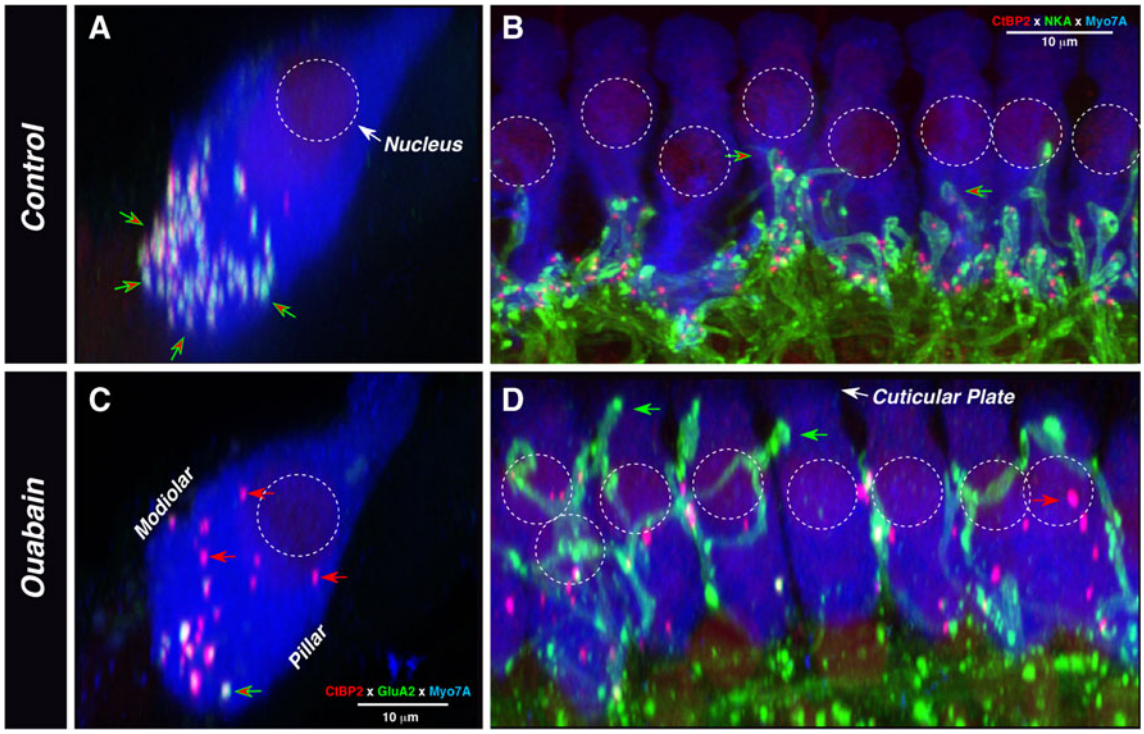

Fig. 5. The location of synaptic elements after ouabain treatment suggests dynamic rearrangement of synaptic architecture in the IHC area. In all images, IHC cytoplasm is stained with anti-myosin VIIA (*blue*). **A**, **C** The double stain for presynaptic ribbons (anti-CtBP2—*red*) and postsynaptic glutamate receptors (*green*) shows that, in the normal ear (**A**), synapses are clustered near the cell's basal pole (*red/green arrows*) and orphan ribbons are rare. After ouabain (**B**), orphan ribbons (*red arrows*) appear throughout the sub- and perinuclear cytoplasm. Both images are from the 32 kHz region and are maximum projections from four adjacent IHCs, acquired as z-stacks with a focal plane parallel to the basilar membrane and then re-projected to mimic radial sections; the ouabain ear was 1 week posttreatment. **B**, **D** The double stain for synaptic ribbons (anti-CtBP2—*red*) and ANF terminals (Na^+/K^+ ATPase—*green*) shows that, in the normal ear (**B**), terminals and associated presynaptic ribbons are confined to the subnuclear region. In the ouabain-treated ear, ectopic terminals climb near the cuticular plate (*green arrows* in **D**), where they are not juxtaposed to ribbons. Numerous orphan ribbons are visible: some are abnormally large (*red arrow*). Control image is from the 11 kHz region; ouabain image is from the 8 kHz region, 1 week posttreatment. Images were acquired as z-stacks with the *x–y* focal plane parallel to the basilar membrane and then re-projected in the *x–z* plane. *Scale bar* in **B** also applies to **D**; *scale bar* in **B** also applies to **A**. Approximate positions of nuclei are shown by *dashed circles* in all panels.

normal DPOAE thresholds as well as suprathreshold amplitudes (data not shown). As seen in Figure 9A, although a >30 dB ABR threshold elevation insures that there has been at least 80 % loss of ANF synapses, a minimal elevation of ABR thresholds does not reliably predict a lack of significant primary neural degeneration. As suggested in prior reports of noise-induced cochlear neuropathy (Kujawa and Liberman, 2009), measures of suprathreshold ABR amplitude (Fig. 9B) are much better at identifying cases with significant loss of ANFs, if the DPOAEs remain normal.

DISCUSSION

Cochlear Neuropathy and Synaptopathy: Ouabain versus Other Insults

In recent years, increasing attention has been paid to the role of primary neural degeneration, i.e., cochlear nerve loss in the absence of hair cell loss, in the overall pathology of acquired sensorineural hearing loss (Kujawa and Liberman, 2009). Several manipulations have been described that selectively destroy cochlear neurons. These include in vivo approaches, i.e., surgical transection of the auditory nerve (Spoendlin and Suter, 1976), moderate-level acoustic overstimulation (Kujawa and Liberman, 2009), and ouabain application to the cochlea's round window membrane (Schmiedt et al., 2002; Lang et al., 2011; Fu et al., 2012), as well as in vitro approaches including perfusion of a cochlear explant with the glutamate analog, kainate (Wang and Green, 2011). All of these neuropathic in vivo manipulations can leave the hair cells intact, suggesting that adult hair cells do not require an afferent innervation to survive. Experiments on cochlear nerve transection show that hair cells can persist for at least 2 years post-denervation (Spoendlin and Suter, 1976).

All these neuropathic manipulations can also be selective for the type-I spiral ganglion cells, the myelinated population of cochlear nerve fibers that

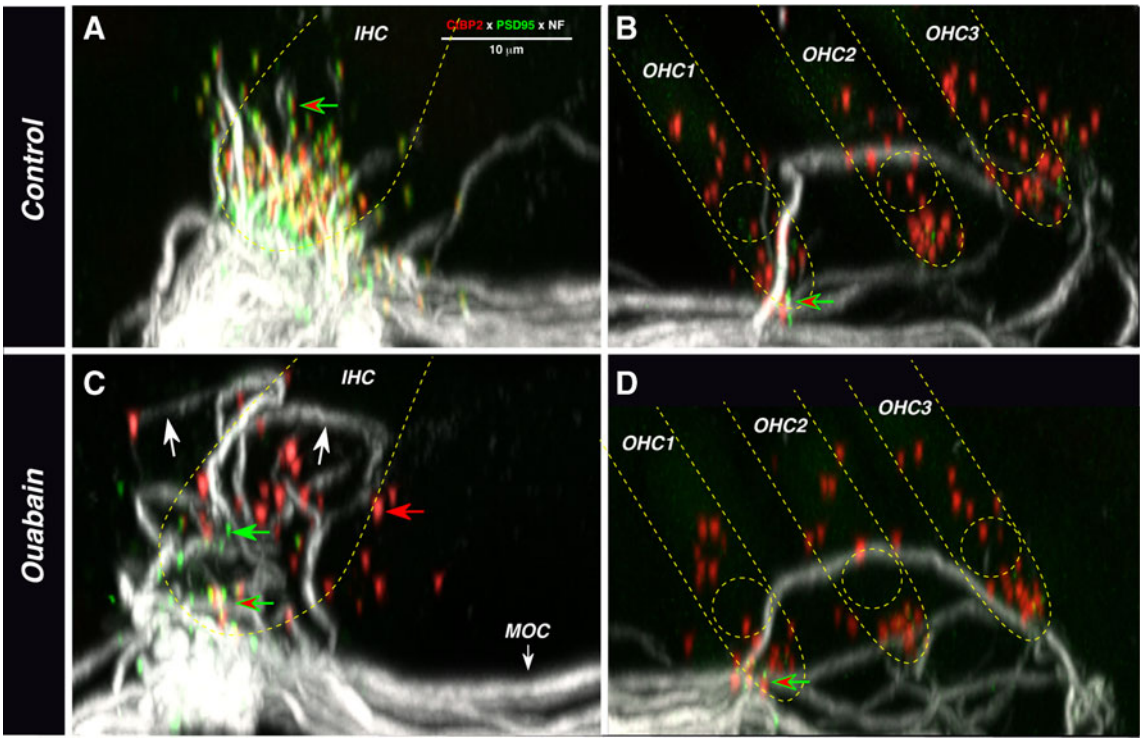

Fig. 6. PSD-95 staining of cochlear whole mounts. **A**, **C** Abnormal terminals in the IHC area of ouabain-treated ears are far from synaptic puncta. IHC area from a control ear (**A**) and a ouabain-treated ear 1 week posttreatment (**C**), viewed as y-z projections. In the control ear, synaptic ribbons (anti-CtBP2: *red*) are almost always juxtaposed to postsynaptic densities (PSD-95: *green*): one is shown at the *red-green arrow*. In the ouabain-treated ear (**C**), there are orphan ribbons (*red arrow*), and orphan PSD-95 patches (*green arrow*), and the ectopic terminals (*white arrows*) are sometimes near ribbons, but never near synapses. **B**, **D** Ouabain has minimal effect on the synaptic architecture in the OHC area: OHC area from the same control and ouabain-treated ears shown in **A** and **C**, respectively. The small number of PSD-95 patches is confined to very basal pole of the OHCs (*red-green arrows*). All image stacks are maximum projections from the 8 kHz region. Each was acquired as a z-stack through ~10 adjacent IHCs, with the *x–y* focal plane parallel to the basilar membrane, and then reprojected to the *y–z* plane to mimic a radial-section view. In each panel, the approximate outlines of hair cell basolateral membranes (and nuclei) are indicated by the *dashed yellow lines*. *Scale bar* in **A** applies to all panels.

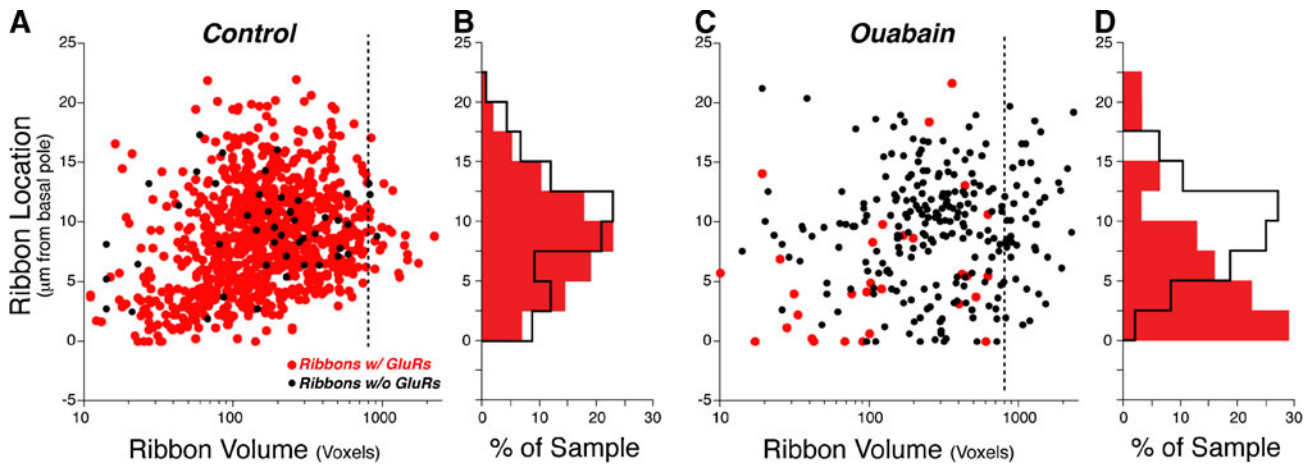

Fig. 7. After ouabain treatment, many IHC ribbons are larger than normal, and most remaining synapses are close to the basal pole of the IHC. Spatial analysis of the synaptic elements derived from 62 IHCs from 3 control ears (**A**, **B**) versus 95 IHCs from 5 ears examined 1 month after ouabain treatment (**C**, **D**). The scatter plots (**A**, **C**) show ribbon position versus ribbon volume (in voxels), with orphan ribbons shown in black. Ribbon position is extracted from image stacks acquired with the *z*-axis perpendicular to the basilar membrane and is defined as the distance (in *z*) from the ribbon closest to the basilar membrane. The *dashed lines* (at volume= 800 voxels) show the increased frequency of large ribbons after ouabain. The location histograms (**B**, **D**) are derived from their respective scatter plots (**A**, **C**) and express location as percent of sample. *Color key* in *panel* **A** applies to all panels. One voxel= 1.439×10^6 nm^3.

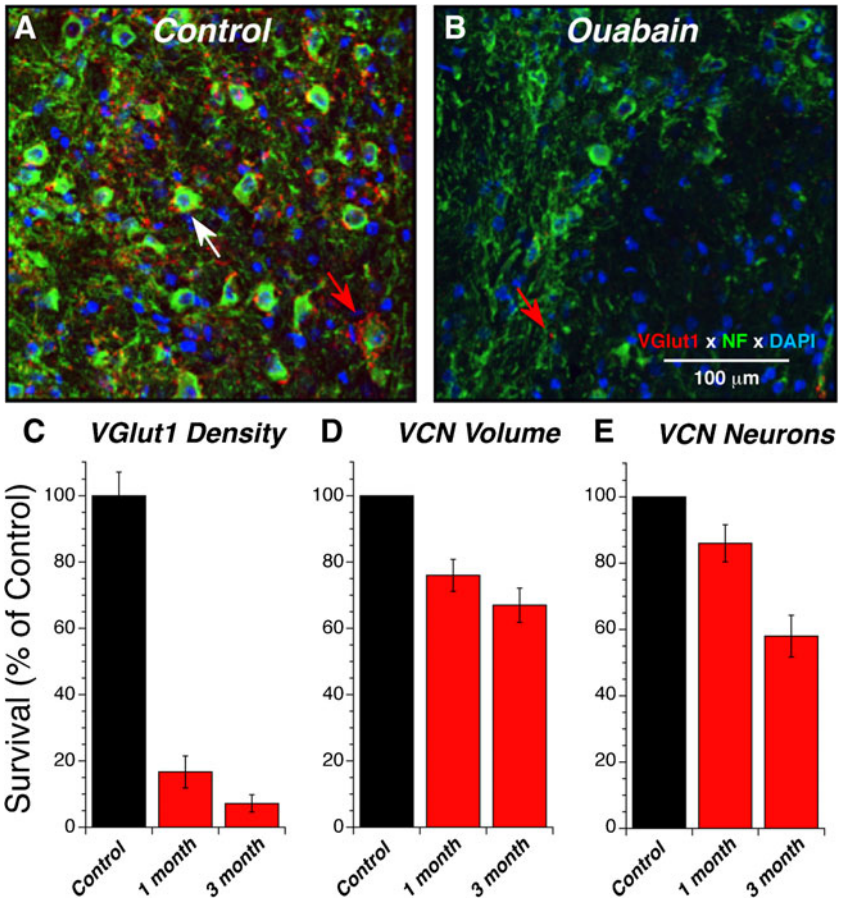

Fig. 8. Analysis of histopathology in the ventral cochlear nucleus (*VCN*) shows a massive loss of ANF projections and a more modest loss of VCN volume and neuronal counts. To assess ANF projections, frozen sections of the VCN (**A**, **B**) were immunostained with anti-VGLUT1 (*red*); immunostaining with anti-neurofilament (NF-*green*) and DAPI (*blue*) was used to count VCN neurons. **C** Quantification of the density of ANF terminals (VGLUT1-positive staining intensity). **D** Quantification of VCN volume. **E** Quantification of VCN neuronal counts. Each metric (**C**, **D**, **E**) is normalized to the mean result from control cases and is based on data from analysis of three sections from each of six control cases, six ouabain cases at 1-month posttreatment survival and six ouabain cases at 3-month posttreatment survival.

synapse exclusively with the IHCs, whereas the normally small population (5 %) of unmyelinated type-II neurons, contacting OHCs, survive in apparently normal numbers (Lang et al., 2005). The survival of type-IIs following kainate or acoustic overexposure may arise because these manipulations cause a type of glutamate excitotoxicity, and type-II neurons do not express the same complement of AMPA-type glutamate receptors as type-Is (Pujol et al., 1985; Liberman et al., 2011). The selective survival of the type-II neurons following ouabain may arise because ouabain-elicited neuronal death is due to blockade of the

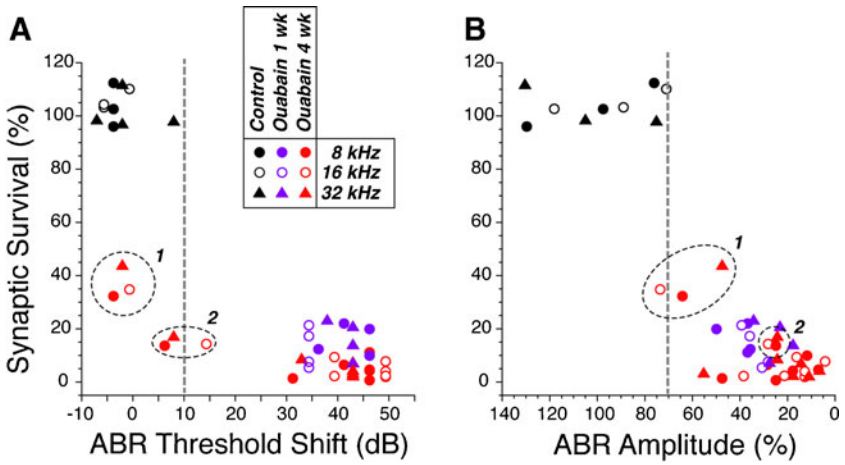

Fig. 9. ABR thresholds (**A**) are a less reliable metric of post-ouabain synaptic survival than suprathreshold ABR amplitudes (**B**). For 3 control and 12 ouabain-treated ears, ABR data were obtained at 8, 16, and 32 kHz and then the ears were processed to count IHC synapses in the same three cochlear regions. Synaptic counts and ABR data are normalized to the mean data at the same frequency region from the control ears. ABR amplitudes are for wave 1 measured in response to tone pips at 80 dB SPL. Two ouabain-treated cases with near-normal ABR thresholds are indicated by the encircled points in each panel: both of these had 1 month posttreatment survival.

α3 subunit of the Na^+/K^+ ATPase (Azarias et al., 2012), and this subunit is expressed by type-I, and not by type-II, spiral ganglion neurons (McLean et al., 2009). The selective survival of type-II neurons following cochlear nerve transection (Spoendlin and Suter, 1976) is not so easily explainable, and therefore suggests that the type-IIs may be generally more robust, perhaps because of a generally lower level of spike activity (Brown, 1994).

Comparison of the cochlear synaptopathy in these neuropathic models reveals both similarities and differences. In the acoustic trauma model, in which the noise exposure is titrated to produce only transient threshold elevation and no loss of hair cells, the ANF terminals retract and the IHC ribbons disappear within 1 day post-exposure, and the degree of synaptopathy remains constant for at least 8 weeks (Kujawa and Liberman, 2009). Although the ouabain model differs in showing a slight increase in ribbon loss from 1 to 12 weeks (Fig. 4), both manipulations produce large numbers of orphan ribbons, many of which appear around the IHC nucleus (compare Figs. 5 here and 4F in (Lin et al., 2011)), and most of which may be deep within the cell cytoplasm rather than tethered to the plasma membrane. In both models, orphan ribbons are still present weeks after the initial neuropathic insult, suggesting either that the degradative processes are very slow, or that there is a continuing production of new ribbons that do not tether to the membrane in the absence of ANF contacts. The in vitro neuropathy model differs from the two in vivo models in that the number of ribbons is only modestly decreased, even up to 3 days after the loss of ANF terminals (Wang and Green, 2011), but is similar in that many of these ribbons are also ectopically positioned near the IHC nucleus. The relative lack of ribbon loss in vitro may reflect the relative immaturity of the cochlear explants, which are extracted from animals around postnatal day 5 (Wang and Green, 2011). All three neuropathy models for which synaptic architecture has been examined are similar in that the synaptic ribbons in the OHC area appear to be unaffected.

Cochlear Neural Repair: Ouabain Versus Other Insults

The issue of whether cochlear synaptic architecture can regenerate is an important biological question with obvious translational relevance. In the neonatal cochlear explant, in vitro, ANF peripheral processes, after retracting to the habenular region in response to kainate application, can regrow and reestablish synapses with IHCs, at least to a limited degree (Wang and Green, 2011). Although it has been claimed that similar regeneration can occur in the kainate-perfused adult cochlea, in vivo, the evidence has been indirect, i.e., threshold recovery of cochlear compound action potentials, coupled with the disappearance of the ANF swelling that is seen immediately after the kainate delivery (Pujol and Puel, 1999). Given that apparently normal thresholds for cochlear gross neural potentials are clearly possible even with massive primary neural degeneration (Fig. 9; also see below), and in the absence of explicit pre- versus post-kainate neuronal counts (Pujol and Puel, 1999), the disappearance of swollen terminals in the kainate model can easily be viewed as due to degeneration rather than regeneration.

In the acoustically traumatized ear, when ANF terminals retract to the habenula, counts of IHC synaptic elements show an immediate post-exposure decline and provide no evidence for synaptogenesis over the next 8 weeks (Kujawa and Liberman, 2009). Similarly, in the present experiments, the synaptic counts only decreased with increasing posttreatment time (Fig. 4), suggesting a lack of synaptogenesis, despite the persistence of a small number of spiral ganglion cells and the persistence of an apparently normal complement of hair cells.

On the other hand, the appearance of ectopic neuronal processes contacting the apical ends of the IHC (Figs. 5D and 6C) suggests a type of neural plasticity in the ouabain neuropathy model, given that such large supranuclear contacts are never seen in the normal mammalian cochlea. Ultrastructural studies of the organ of Corti up to 2 years after cochlear nerve section have also noted the appearance of "giant fibers" in the IHC area (Spoendlin and Suter, 1976). The nerve-section study also observed numerous large myelinated fibers traversing the denuded spiral ganglion without connecting to a spiral ganglion cell, and suggested that these giant fibers might represent new branches from the olivocochlear bundle rather than from the cochlear nerve. The neural immunomarkers used in the present study, i.e., neuron-specific tubulin (TuJ), neurofilament, and Na^+/K^+ ATPase α3, all stain both type-I afferents and MOC efferents, thus the origin of these aberrant fibers remains unclear. However, an olivocochlear origin might "explain" why these regenerated nerve terminals fail to form ribbon synapses with the IHCs they contact.

ABRs and the Quantitative Assessment of Cochlear Neuropathy

The ability to selectively destroy cochlear nerve fibers without damaging the hair cells is useful for animal experiments designed to test the efficacy of neural regeneration strategies in the ear as well as to parse the relative contributions of hair cell versus neural damage to the complex perceptual anomalies that

comprise sensorineural hearing loss. For both these purposes, the animal model is most powerful if, in addition to hair cell survival, the hair cells are also undamaged and therefore functioning normally.

Measurement of DPOAEs can provide a sensitive measure of the functional state of the outer hair cells (as well as the stria vascularis and other "presynaptic" structures in the inner ear). Although prior studies have shown that DPOAEs in response to moderate-level primary tones (50 dB SPL) are unchanged after a neuropathic ouabain treatment (Lang et al., 2005), this is the first study to demonstrate that DPOAEs at "threshold" levels (<20 dB SPL primaries) can also be unaffected (Fig. 1) by a drug treatment that eliminates virtually all synapses from the IHC area (Fig. 4). This suggests that the outer hair cells are indeed functioning normally.

Evidence that the inner hair cells are also functioning normally is provided by the ABR waveforms recorded post-ouabain treatment (Fig. 1C). Prior reports in mutant mice lacking synaptic ribbons (Buran et al., 2010) and in humans (Santarelli et al., 2009) or mice (Pangrsic et al., 2010) with mutations in the gene for otoferlin, which is necessary for normal synaptic release in the IHC, both show ABR waveform abnormalities strikingly similar to those shown here, i.e., reduction or elimination of a normal wave 1 with a selective sparing of the short-latency shoulder on its rising phase. Together with the present report, these observations provide strong support for the notion that this early potential is the equivalent of the (presynaptic) "summating potential" recorded at the round window, i.e., the far-field sum of the hair cell receptor potentials (Durrant et al., 1998). Since this potential is dominated by the IHCs (Durrant et al., 1998), its normal amplitude in the post-ouabain ears (Fig. 1C) strongly suggests that IHC function also remains normal.

If hair cell function is normal, the degree of (primary) cochlear nerve degeneration or dysfunction should be proportional to ABR amplitudes, with accuracy limited only by the inter-animal variance of these far-field neural potentials. Present results suggest that ABR amplitudes are indeed a more robust indicator of graded neuropathy than ABR thresholds (Fig. 9). The idea that far-field cochlear neural thresholds are remarkably insensitive to neural degeneration (see Fig. 9A) has been noted before, both for the ABR, in studies of noise-induced primary neural degeneration (Kujawa and Liberman, 2009) and for the compound action potential in studies of carboplatin-induced selective IHC loss (Liberman et al., 1997). This is partially explained by considering that ABR thresholds (~30 dB SPL) are significantly higher than single-fiber thresholds (~0 dB SPL (Taberner and Liberman, 2005)); thus, an additional 10 dB increase to ~40 dB SPL by impinging on the more broadly tuned portions of ANF tuning curves, rapidly recruits ANFs over large extents of the cochlear spiral. For ABRs, another contributing factor is that a peripheral neuropathy may enhance responses in the central auditory nuclei, such as cochlear nucleus and the inferior colliculus (Mulders and Robertson, 2009; Vogler et al., 2011), which contribute to the later waves that typically appear at lower SPLs than wave 1. Indeed, post-exposure decreases in ABR thresholds, without parallel changes in DPOAE thresholds, have been noted in the acoustic trauma model of neuropathy (Fig. 2B in (Kujawa and Liberman, 2009)).

The apparent lack of spontaneous synaptogenesis in the adult IHC area after ouabain treatment, and the near complete loss of synaptic terminals that is achievable without damaging the hair cells, make this model a powerful platform on which to test the ability of neural progenitors to re-innervate a denervated organ of Corti. The ability to titrate the damage to produce subtotal denervation, again without apparent hair cell damage, also make this a powerful model system to study the role of neuropathy per se in the generation of central hyperactivity following peripheral insult; a condition that has been implicated in the generation of both tinnitus and hyperacusis.

ACKNOWLEDGMENTS

This work was supported by grants from the National Institute on Deafness and other Communicative Disorders: RO1 DC007174 (AE), R01 DC 00188 (MCL), R01 DC009836 (DBP), and P30 DC05209 (MCL).

REFERENCES

AZARIAS G, KRUUSMAGI M, CONNOR S, AKKURATOV EE, LIU XL, LYONS D, BRISMAR H, BROBERGER C, APERIA A (2012) A specific and essential role for Na,K-ATPase alpha3 in neurons co-expressing alpha1 and alpha3. J Biol Chem.

BROWN MC (1994) Antidromic responses of single units from the spiral ganglion. J Neurophysiol 71:1835–1847

BURAN BN, STRENZKE N, NEEF A, GUNDELFINGER ED, MOSER T, LIBERMAN MC (2010) Onset coding is degraded in auditory nerve fibers from mutant mice lacking synaptic ribbons. J Neurosci 30:7587–7597

CHEN W, JONGKAMONWIWAT N, ABBAS L, ESHTAN SJ, JOHNSON SL, KUHN S, MILO M, THURLOW JK, ANDREWS PW, MARCOTTI W, MOORE HD, RIVOLTA MN (2012) Restoration of auditory-evoked responses by human ES-cell-derived otic progenitors. Nature 490:278–282

CORRALES CE, PAN L, LI H, LIBERMAN MC, HELLER S, EDGE AS (2006) Engraftment and differentiation of embryonic stem cell-derived neural progenitor cells in the cochlear nerve trunk: growth of processes into the organ of Corti. J Neurobiol 66:1489–1500

DURRANT JD, WANG J, DING DL, SALVI RJ (1998) Are inner or outer hair cells the source of summating potentials recorded from the round window? J Acoust Soc Am 104:370–377

FRANK T, RUTHERFORD MA, STRENZKE N, NEEF A, PANGRSIC T, KHIMICH D, FEJTOVA A, GUNDELFINGER ED, LIBERMAN MC, HARKE B, BRYAN KE, LEE A, EGNER A, RIEDEL D, MOSER T (2010) Bassoon and the synaptic ribbon organize Ca(2)+channels and vesicles to add release sites and promote refilling. Neuron 68:724–738

FU Y, DING D, JIANG H, SALVI R (2012) Ouabain-induced cochlear degeneration in rat. Neurotox Res 22:158–169

KHIMICH D, NOUVIAN R, PUJOL R, TOM DIECK S, EGNER A, GUNDELFINGER ED, MOSER T (2005) Hair cell synaptic ribbons are essential for synchronous auditory signaling. Nature 434:889–894

KUJAWA SG, LIBERMAN MC (2009) Adding insult to injury: cochlear nerve degeneration after "temporary" noise-induced hearing loss. J Neurosci 29:14077–14085

LANG H, SCHULTE BA, SCHMIEDT RA (2005) Ouabain induces apoptotic cell death in type I spiral ganglion neurons, but not type II neurons. J Assoc Res Otolaryngol 6:63–74

LANG H, SCHULTE BA, GODDARD JC, HEDRICK M, SCHULTE JB, WEI L, SCHMIEDT RA (2008) Transplantation of mouse embryonic stem cells into the cochlea of an auditory-neuropathy animal model: effects of timing after injury. J Assoc Res Otolaryngol 9:225–240

LANG H, LI M, KILPATRICK LA, ZHU J, SAMUVEL DJ, KRUG EL, GODDARD JC (2011) Sox2 upregulation and glial cell proliferation following degeneration of spiral ganglion neurons in the adult mouse inner ear. J Assoc Res Otolaryngol 12:151–171

LAWNER BE, HARDING GW, BOHNE BA (1997) Time course of nerve-fiber regeneration in the noise-damaged mammalian cochlea. Int J Dev Neurosci 15:601–617

LIBERMAN MC (1982) Single-neuron labeling in the cat auditory nerve. Science 216:1239–1241

LIBERMAN MC, CHESNEY CP, KUJAWA SG (1997) Effects of selective inner hair cell loss on DPOAE and CAP in carboplatin-treated chinchillas. Audit Neurosci 3:255–268

LIBERMAN LD, WANG H, LIBERMAN MC (2011) Opposing gradients of ribbon size and AMPA receptor expression underlie sensitivity differences among cochlear-nerve/hair-cell synapses. J Neurosci 31:801–808

LIN HW, FURMAN AC, KUJAWA SG, LIBERMAN MC (2011) Primary neural degeneration in the Guinea pig cochlea after reversible noise-induced threshold shift. J Assoc Res Otolaryngol 12:605–616

MATSUBARA A, LAAKE JH, DAVANGER S, USAMI S, OTTERSEN OP (1996) Organization of AMPA receptor subunits at a glutamate synapse: a quantitative immunogold analysis of hair cell synapses in the rat organ of Corti. J Neurosci 16:4457–4467

MCLEAN WJ, SMITH KA, GLOWATZKI E, PYOTT SJ (2009) Distribution of the Na, K-ATPase alpha subunit in the rat spiral ganglion and organ of Corti. J Assoc Res Otolaryngol 10:37–49

MEYER AC, FRANK T, KHIMICH D, HOCH G, RIEDEL D, CHAPOCHNIKOV NM, YARIN YM, HARKE B, HELL SW, EGNER A, MOSER T (2009) Tuning of synapse number, structure, and function in the cochlea. Nat Neurosci 12:444–453

MULDERS WH, ROBERTSON D (2009) Hyperactivity in the auditory midbrain after acoustic trauma: dependence on cochlear activity. Neuroscience 164:733–746

MULLER M, VON HUNERBEIN K, HOIDIS S, SMOLDERS JW (2005) A physiological place-frequency map of the cochlea in the CBA/J mouse. Hear Res 202:63–73

OPAZO P, SAINLOS M, CHOQUET D (2012) Regulation of AMPA receptor surface diffusion by PSD-95 slots. Curr Opin Neurobiol 22:453–460

PANGRSIC T, LASAROW L, REUTER K, TAKAGO H, SCHWANDER M, RIEDEL D, FRANK T, TARANTINO LM, BAILEY JS, STRENZKE N, BROSE N, MULLER U, REISINGER E, MOSER T (2010) Hearing requires otoferlin-dependent efficient replenishment of synaptic vesicles in hair cells. Nat Neurosci 13:869–876

PUJOL R, PUEL JL (1999) Excitotoxicity, synaptic repair, and functional recovery in the mammalian cochlea: a review of recent findings. Ann N Y Acad Sci 884:249–254

PUJOL R, LENOIR M, ROBERTSON D, EYBALIN M, JOHNSTONE BM (1985) Kainic acid selectively alters auditory dendrites connected with cochlear inner hair cells. Hear Res 18:145–151

SANTARELLI R, DEL CASTILLO I, RODRIGUEZ-BALLESTEROS M, SCIMEMI P, CAMA E, ARSLAN E, STARR A (2009) Abnormal cochlear potentials from deaf patients with mutations in the otoferlin gene. J Assoc Res Otolaryngol 10:545–556

SCHMIEDT RA, OKAMURA HO, LANG H, SCHULTE BA (2002) Ouabain application to the round window of the gerbil cochlea: a model of auditory neuropathy and apoptosis. J Assoc Res Otolaryngol 3:223–233

SPOENDLIN H, SUTER R (1976) Regeneration in the VIII nerve. Acta Otolaryngol 81:228–236

STAMATAKI S, FRANCIS HW, LEHAR M, MAY BJ, RYUGO DK (2006) Synaptic alterations at inner hair cells precede spiral ganglion cell loss in aging C57BL/6J mice. Hear Res 221:104–118

STANKOVIC K, RIO C, XIA A, SUGAWARA M, ADAMS JC, LIBERMAN MC, CORFAS G (2004) Survival of adult spiral ganglion neurons requires erbB receptor signaling in the inner ear. J Neurosci 24:8651–8661

STARR A, PICTON TW, SININGER Y, HOOD LJ, BERLIN CI (1996) Auditory neuropathy. Brain 119(Pt 3):741–753

TABERNER AM, LIBERMAN MC (2005) Response properties of single auditory nerve fibers in the mouse. J Neurophysiol 93:557–569

VOGLER DP, ROBERTSON D, MULDERS WH (2011) Hyperactivity in the ventral cochlear nucleus after cochlear trauma. J Neurosci 31:6639–6645

WANG Q, GREEN SH (2011) Functional role of neurotrophin-3 in synapse regeneration by spiral ganglion neurons on inner hair cells after excitotoxic trauma in vitro. J Neurosci 31:7938–7949

ZHOU J, NANNAPANENI N, SHORE S (2007) Vesicular glutamate transporters 1 and 2 are differentially associated with auditory nerve and spinal trigeminal inputs to the cochlear nucleus. J Comp Neurol 500:777–787